Magnetic Bistability and Controllable Reversal of Asymmetric Ferromagnetic Nanorings

F. Q. Zhu,[1] G. W. Chern,[1] O. Tchernyshyov,[1] X. C. Zhu,[2] J. G. Zhu,[2] and C. L. Chien[1,*]

[1]*Department of Physics and Astronomy, Johns Hopkins University, Baltimore, Maryland 21218, USA*

[2]*Department of Electrical and Computer Engineering, Carnegie-Mellon University, Pittsburgh, Pennsylvania 15213, USA*

(Received 9 August 2005; published 17 January 2006)

Magnetization reversals through the formation of a vortex state and the rotation of an onion state are two processes with comparable probabilities for symmetric magnetic nanorings with a radius of about 50 nanometers. This magnetic bistability is the manifestation of the competition between the exchange energy and the magnetostatic energy in nanomagnets. The relative probability of the two processes in symmetric nanorings is dictated by the ring geometry and cannot be altered after fabrication. In this work, we report a novel type of nanorings—asymmetric nanorings. By tuning the asymmetry, we can control the fraction of the vortex formation process from about 40% to nearly 100% by utilizing the direction of the external magnetic field. The observed results have been accounted for by the dependence of the domain-wall energy on the local cross-section area for which we have provided theoretical calculations.

DOI: 10.1103/PhysRevLett.96.027205 PACS numbers: 75.75.+a, 75.30.Kz, 75.70.Kw, 81.07.−b

The magnetic configurations and reversal mechanisms of nanomagnets depend intricately on their geometrical shapes and sizes and the competition between the magnetostatic and the exchange energies. For example, an elongated nanomagnet normally acquires the single-domain state with magnetic poles and stray magnetic fields. More interestingly, a circular magnetic disk can acquire the vortex state in which the magnetization forms a closure structure without magnetic poles or stray fields [1–3]. This occurs in disks of sufficiently large radius r where the magnetostatic energy prevails at the expense of the exchange energy. There is, however, a vortex core that tends to disrupt the vortex state in disks with decreasing r. Indeed, when r is below a threshold value r_c, which for Co and permalloy disks are in the range of a few hundred nanometers [4], the vortex state cannot be accommodated. The bistability of the single-domain state and the vortex state in Co nanodots has recently been reported [5].

A more intriguing geometry is that of a magnetic nanoring which has no central area and, therefore, contains no vortex core in the vortex state [6–15]. As a result, the vortex state can be stably retained in nanorings of even very small r. Ideal nanorings must have not only well-defined inner and outer radii but also a narrow width less than that of a domain wall (DW, about 50 nm in Co) to ensure that no vortex core can exist within the ring width. These requirements are challenging even for advanced electron-beam lithography, which has been commonly used for fabricating nanorings [6–11]. The difficulty is further compounded by the need for a large number of nanorings for most measurements. Recently, we reported a new method using nanospheres as templates for the fabrication of a large number (10^9) of magnetic nanorings with $r = 50$ and 20 nm in ring width [16]. These nanorings with $r = 50$ nm offer a new and hitherto unavailable medium for exploring the intricate magnetic properties of nanorings. Nanorings have also been proposed for applications in high density magnetic recording and vertical magnetic random access memory [17].

The remnant state (at $H = 0$) of a magnetic nanoring after saturation is the so-called "onion" state, consisting of two domains with semicircular magnetizations of different helicity separated by two DWs on the opposite sides [6]. Micromagnetic simulation based on the Landau-Lifshitz-Gilbert equation and experimental studies have revealed that, under a magnetic field in the opposite direction, the onion state can switch via two different processes as shown in Fig. 1 [16]. If the two DWs move towards each other in the beginning [Fig. 1(a)], they will be driven by the external field to move closer until annihilation to form the vortex state. If the two DWs move in opposite directions in the beginning, however, they will continue to do so until the onion state is fully reversed, as illustrated in Fig. 1(b). These two processes are called the vortex formation process (V process) and the onion rotation process (O process), respectively. The probability P of the V process, defined as the probability that a nanoring switches through the formation of a vortex state, depends on both the radius and the wall width of the ring [18]. For a large ring with r in the micrometer range, the V process is dominant, whereas

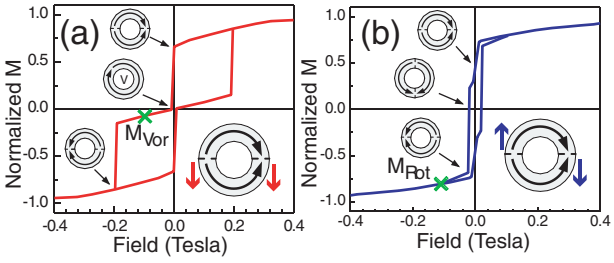

FIG. 1 (color online). Micromagnetic simulation of (a) the vortex formation process and (b) the onion rotation process. Average magnetizations M_{Vor} and M_{Rot} in the middle of the two switching fields are indicated by cross symbols. Insets illustrate the motion of domain walls at the onset of reversal.

for r in the 50 nm range, the two reversal processes have comparable probability. The value of P can be determined by analyzing the hysteresis loops which are superpositions of the two types of loops. One notes that the bistability here is between the V process and the O process, whereas in nanodots [5] it is between the single-domain state and the vortex state.

It is important to understand the movement of DWs in nanorings to predictably achieve the vortex state, a feat also essential for applications of magnetic nanorings. In this Letter, we report the special features of a new type of nanorings, which are *asymmetric* in the cross section. We show that the fraction P of the V process can be controlled by the direction of external field with respect to the axis of the asymmetric nanorings. In particular, when the magnetic field is applied along the asymmetry axis, the fraction P is nearly 100%. We have also developed a theoretical model to account for the preferred vortex formation reversal mechanism. The introduction of asymmetry in the nanorings allows full vortex formation without losing the virtues of small dimension, high stability, and high areal density.

We used $r = 50$ nm polystyrene (PS) spheres as the templates (Fig. 2). A monolayer of isolated PS spheres were chemically attached to a Si(100) surface. A 40 nm thick Co film was sputter-deposited from a 99.995% pure Co target in a magnetron sputtering system with an *in situ* substrate tilting-angle adjusting capability. The base pressure and Ar sputtering pressure are 6×10^{-8} torr and 6 mtorr, respectively. The substrates were swept across the sputtering plasma in order to have a uniform thickness everywhere. A broad beam Ar^+ ion source was then used to etch away all Co except those protected under the PS spheres resulting in Co nanorings. When the ion beam was at normal incidence [$\alpha = 0$, Fig. 2(b)], nanorings of uniform width, or symmetric nanorings, were obtained. However, when the substrate was tilted by an angle α as shown in Fig. 2(c), asymmetric nanorings were obtained. A capping layer of 5 nm Au was deposited for protection against oxidation. Nanorings fabricated with $\alpha < 10°$ show less asymmetry, whereas those with α much larger than 14° become connected due to the shadowing effects of the PS spheres. In the following, asymmetric nanorings fabricated with $a = 10^{\circ}$ and 14° are denoted as AR10 and AR14, respectively.

Figures 2(d) and 2(e) are the top view scanning electron micrographs (SEM) of the symmetric and asymmetric nanorings, respectively. The cross-section area in the symmetric nanoring is constant along the circumference but varies in sample AR14, with the left side much wider and thicker than the right side. The asymmetry of AR14 is also revealed in the inset in Fig. 2(e) taken with a composition sensitive detector. The maximum and minimum ring widths of AR14 are about 60 and 10 nm, respectively.

The magnetic switching properties were measured with an ADE model 10 vector vibrating sample magnetometer at room temperature. To reveal the effect of asymmetry on

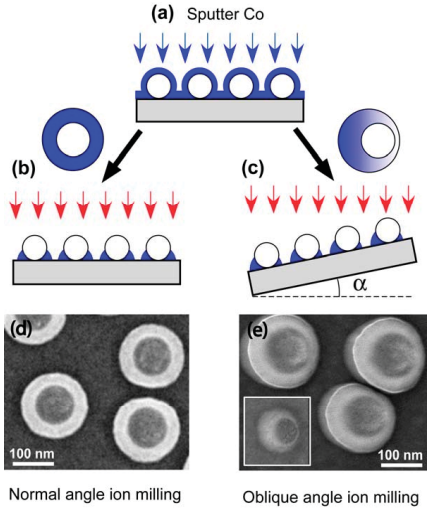

FIG. 2 (color online). Fabrication schematics of nanorings. (a) Si substrate attached with a layer of PS spheres is etched by Ar^+ ion beam at (b) a normal angle for normal nanorings and at (c) an oblique angle for asymmetric ones. A protective capping layer of Au is sputtered at the last step. Top view SEM micrographs of (d) symmetric and (e) asymmetric nanorings fabricated from $r = 50$ nm PS spheres at 0° and 14° ion milling angles. Shading in the diagram represents thickness variation. Inset: Composition sensitive SEM image of the ring; bright areas represent Co.

switching properties, measurements were made with the magnetic field applied in the substrate plane along different angle θ (bottom right inset in Fig. 3, pointing from A to A'). Ten hysteresis loops of sample AR14 measured at $\theta = 0^{\circ}$ to 90° are plotted together in Fig. 3, all showing the two-step switching characteristics but with a systematic variation as θ is varied. The highlighted area represents the field range in which the magnetization has substantial changes when the field angle varies. For comparison, the top left inset shows that the hysteresis loops of the symmetric nanorings are independent of θ as expected.

The measured hysteresis loops were analyzed using the two simulated switching loops as shown in Fig. 1 to determine the fractions of the two processes. The V process shows two switching fields, between which the ring retains the vortex state. The magnetization of the vortex state in a magnetic field increases weakly from 0 due to the slight tilting of the moments by the external field. The average normalized magnetization of the vortex state M_{Vor} [indicated by the cross in Fig. 1(a)] between the two switching fields is, therefore, not zero but a small finite value ($\approx$0.0795). However, the O process shows one-step reversal, and the average normalized magnetization $M_{\mathrm{Rot}} \approx 0.862$ [indicated by the cross in Fig. 1(b)] at the same field is large and close to the saturation magnetization. When both processes are present as in a collection of nanorings, the resultant hysteresis loop is the superposition of these two loops weighted by the fractions P and 1-P respectively. Consequently, the overall corresponding average magnetization will be $M_{\mathrm{mid}} = P \times M_{\mathrm{Vor}} + (1 - P) \times M_{\mathrm{Rot}}$. In

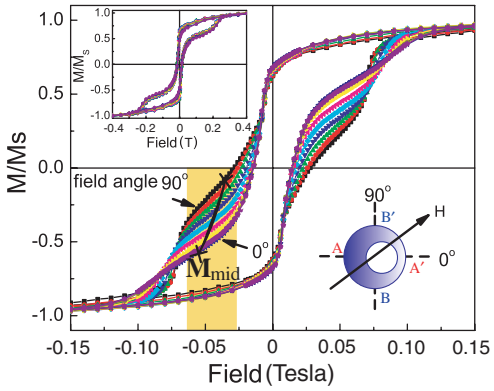

FIG. 3 (color). Evolution of hysteresis loops of $r = 50$ nm asymmetric nanorings at various magnetic field directions between 0° (innermost curve) and 90° (outermost curve). The highlighted area represents the field range in which the magnetization has substantial changes. Bottom right inset: The symmetry axis is defined as the direction pointing from the widest part A to the thinnest part A'; the asymmetry axis is 90° away from it, from B to B'. Shading represents thickness variation. Top left inset: Hysteresis loops of the uniform nanorings measured along various in-plane field directions are essentially the same.

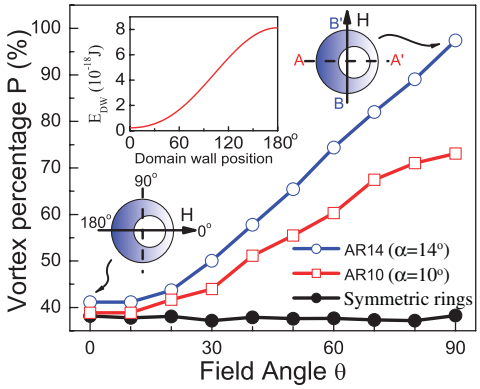

FIG. 4 (color online). Field angle dependence of the probability P of the vortex formation process for symmetric nanorings (solid dots), asymmetric nanorings AR10 (milling angle = 10°, open squares), and AR14 (milling angle = 14°, open circles). The connecting lines are a guide for the eyes. Inset: Energy of domain wall E changes with the angular position of the domain wall, with the maxima and minima at 180° and 0°, respectively.

Fig. 3, the location of M_{Mid}, indicated by the black line, depends systematically on the field direction. When the magnetic field direction is changed from the symmetry axis ($\theta = 0°$) to the asymmetry axis ($\theta = 90°$), M_{Mid} decreases progressively. The fraction P can be deduced as $P = (M_{\mathrm{Rot}} - M_{\mathrm{Mid}})/(M_{\mathrm{Rot}} - M_{\mathrm{Vor}})$ from the above formula. The derived values of P in symmetric nanorings and asymmetric nanorings of AR10 and AR14 are plotted together in Fig. 4 as a function of the field angle θ. In symmetric nanorings, P is about 38% and does not depend on the field direction. However, for asymmetric nanorings, the value of P shows a strong dependence on the field direction, which changes from 39% to 73% in AR10 and from 41% to 98% in AR14. Therefore, we not only have observed the magnetic bistability of the asymmetric nanorings but also have achieved tuning of the bistability with the direction of the external field. The value of $P = 98\%$ at $\theta = 90°$ for AR14 shows that nearly every nanoring reverses its magnetization through the V process, an important attribute for applications.

The fraction P for the V process is a direct measure of the magnetic bistability. In very large rings where the magnetostatic energy dominates, only the V process occurs ($P = 1$). In the other extreme of very small rings where exchange energy dominates, the magnetic reversal undergoes only the O process ($P = 0$). For the intermediate sizes of a few hundred nanometers, both processes can occur with certain probabilities. The motion of DWs at the onset of the magnetization reversal determines the type of the reversal process, as shown by the insets in Fig. 1. For a symmetric nanoring with a constant cross section, P is intrinsic to its dimension and cannot be altered. In contrast, in asymmetric nanorings P can be varied greatly by exploiting the field angle. In the following, we address the effects of cross-section area on the switching behavior of asymmetric nanorings.

The key aspect is to determine the dependence of the domain-wall energy E on the local cross-section area of the nanoring. To this end, we use a straight strip of constant width w and thickness t to approximate one segment of the ring and consider the energy E of a domain wall inside. The general trend is that E increases with both w and t. Even in the absence of intrinsic anisotropy in the material, the problem is computationally difficult because of the long-range magnetostatic interaction. When the ring is thin and narrow, the computation simplifies in the thin-film limit of $t \ll w$ and $tw \ll \lambda^2 \ll wt\log(w/t)$, where $\lambda = \sqrt{A/\mu_0 M_0^2}$ is the magnetic length (3.8 nm in Co) [19,20]. In this geometry, the magnetostatic term becomes local, making an analytical solution possible. Owing to the shape anisotropy, the magnetization lies in the plane of the film. The magnetic energy is the sum of the exchange and the magnetostatic terms:

$$E[\hat{\mathbf{m}}(r)] = \int_{\Omega} |\nabla \hat{\mathbf{m}}|^2 d^2 r + (1/\Lambda) \int_{\partial\Omega} (\hat{\mathbf{m}} \cdot \hat{\mathbf{n}})^2 dr, \quad (1)$$

where $\hat{\mathbf{m}} = (\cos(\theta), \sin(\theta))$ is a unit vector depicting the in-plane components of the magnetization, $\hat{\mathbf{n}} = (0, 1)$ is the normal to the edge, $\Lambda = \lambda^2/t\log(w/t)$ is the thin-film magnetic length [16,17], Ω is the two-dimensional strip $-w/2 < y/w/2$, and $\partial\Omega$ is its boundary. The energy is made dimensionless by dividing out the unit of energy $\mu_0 M_0^2 \lambda^2 t = At$. Equation (1) is, in fact, the familiar XY model with anisotropy at the edge added by the magnetostatic term. The ground states are uniform with $\theta = 0$ or π.

Minimization of the energy [Eq. (1)] yields the Laplace equation $\nabla^2\theta = 0$ and the boundary conditions $\partial_y\theta = \mp(1/\Lambda)\sin 2\theta$ at the upper and lower edges $y = \pm w/2$.

A domain-wall solution interpolating between the ground states has the following structure:

$$\tan\theta(x, y) = \cos ky / \sinh k(x - X), \quad (2)$$

where X is the horizontal coordinate of the wall and the wave vector k is determined by the boundary conditions. In the thin-film limit, $k \approx \pi/(w + 2\Lambda)$. The energy [Eq. (1)] of the domain wall evaluates to $E \approx 2\pi(1 + \log(w/\pi\Lambda))$. As expected for the XY model, the exchange energy depends logarithmically on the strip width w and on the short-distance cutoff Λ. After restoring the energy units and expressing Λ in terms of the relevant parameters, we obtain the final result for the energy of the domain wall

$$E_{\mathrm{DW}} \approx 2\pi A t \log\left(\frac{ewt\log(w/t)}{\pi\lambda^2}\right). \quad (3)$$

Note that, in the thin-film limit, where exchange energy dominates, the energy of the domain wall depends most sensitively (linearly) on the thickness t of the strip, whereas the dependence on the width w is rather weak (logarithmic). Our numerical evaluation and dimensional analysis [21] show that, in thicker and wider rings, E is still an increasing function of w and t. Every small segment of the asymmetrical nanoring can be approximated as a straight strip. We can then apply Eq. (3) to estimate the domain-wall energy inside the nanorings.

In asymmetric nanorings, the ring width and thickness vary along the circumference, with their minima and maxima separated by 180°. DW energy $E(\theta)$, therefore, changes with the angular position θ of the DW as plotted in the inset of Fig. 4. If the initial magnetic field is along the symmetry axis (AA'), one DW (DMW1) will be generated at the thinnest location A and the other DW (DMW2) at the thickest location A' after the field is removed (Fig. 3). Under a reversal magnetic field, DMW1 and DMW2 still have two possible directions to move, and the situation is not very different from that of the symmetric rings. The vortex probability P is close to that of a uniform nanoring. However, if the initial field is along the asymmetry axis (BB'), DMW1 and DMW2 will be generated at the middle locations B and B' with the largest slope. Both domain walls tend to slide to the same energy minimum position A' hindered only by the pinning forces of the local defects and roughness. As a consequence, the V process is enhanced. The higher the asymmetry and the larger the geometrical slope, the higher P is, as shown in Fig. 4.

Imposing additional anisotropy into the rings and disks to break the circular symmetry has been previously reported [7–9,22,23]. These include creating two notches at the opposite ends in the rings as local DW pinning centers [8,9] and fabricating elliptical rings [7]. However, these schemes introduce anisotropy only in one axis. Furthermore, the large sizes (micrometers) of the rings also deprive the observation of the onion rotation process. In contrast, for the asymmetrical nanorings in this work, the much smaller size of 100 nm allows the observation of the onion rotation process. More importantly, we have created a nonlocal and continuously varying anisotropy by changing the nanoring cross section along the circumference. As a result, we can control the fractions of the vortex and the rotating-onion processes solely by the direction of the applied magnetic field.

In summary, we have observed the magnetic bistability between the V process and the O process of asymmetric nanorings fabricated with oblique angle ion beam etching. Comparing with the symmetric nanorings, asymmetric nanorings have controllable magnetic switching properties depending on the direction of the external field. We have achieved nearly 100% vortex reversal in the asymmetric nanorings, while the symmetric nanorings can accommodate only 40%. We have also computed the energy of the DW, which depends on the local thickness linearly. The variation of the local cross section in asymmetric nanoring favors the DW motion towards the thinnest position, thus enhancing the V process.

This work has been supported by NSF Grant No. DMR05-20491.

*Corresponding author.
Electronic address: clc@pha.jhu.edu

[1] T. Shinjo *et al.*, Science **289**, 930 (2000).
[2] A. Wachowiak *et al.*, Science **298**, 577 (2002).
[3] S. B. Choe *et al.*, Science **304**, 420 (2004).
[4] R. P. Cowburn *et al.*, Phys. Rev. Lett. **83**, 1042 (1999).
[5] H. F. Ding *et al.*, Phys. Rev. Lett. **94**, 157202 (2005).
[6] J. Rothman *et al.*, Phys. Rev. Lett. **86**, 1098 (2001).
[7] F. J. Castaño, C. A. Ross, and A. Eilez, J. Phys. D **36**, 2031 (2003).
[8] M. Kläui *et al.*, Appl. Phys. Lett. **78**, 3268 (2001).
[9] M. Kläui *et al.*, Appl. Phys. Lett. **81**, 108 (2002).
[10] X. B. Zhu *et al.*, J. Appl. Phys. **93**, 8540 (2003).
[11] S. P. Li *et al.*, Phys. Rev. Lett. **86**, 1102 (2001).
[12] K. L. Hobbs *et al.*, Nano Lett. **4**, 167 (2004).
[13] W. L. Zhou *et al.*, J. Appl. Phys. **93**, 7340 (2003).
[14] S. L. Tripp, S. V. Pusztay, A. E. Ribbe, and A. Wei, J. Am. Chem. Soc. **124**, 7914 (2002).
[15] X. Y. Kong, Y. Ding, R. Yang, and Z. L. Wang, Science **303**, 1348 (2004).
[16] F. Q. Zhu *et al.*, Adv. Mater. **16**, 2155 (2004).
[17] J.-G. Zhu, Y. Zheng, and G. A. Prinz, J. Appl. Phys. **87**, 6668 (2000).
[18] F. Q. Zhu and C. L. Chien (to be published).
[19] R. V. Kohn and V. V. Slastikov, Proc. R. Soc. A **460**, 1 (2004).
[20] M. Kurzke, Max Planck Institute for Mathematics in the Sciences Report No. 14/2004, 2004 (to be published).
[21] O. Tchernyshyov and G.-W. Chern, Phys. Rev. Lett. **95**, 197204 (2005).
[22] J. Sort *et al.*, Phys. Rev. Lett. **95**, 067201 (2005).
[23] Johannes Eisenmenger *et al.*, Phys. Rev. Lett. **94**, 057203 (2005).